Neutron diffuse scattering in deuterated *para*-terphenyl, $C_{18}D_{14}$

2009 J. Phys.: Condens. Matter 21 124204

(http://iopscience.iop.org/0953-8984/21/12/124204)

J. Phys.: Condens. Matter **21** (2009) 124204 (10pp) doi:10.1088/0953-8984/21/12/124204

Neutron diffuse scattering in deuterated *para*-terphenyl, $C_{18}D_{14}$

D J Goossens[1,2,5], A G Beasley[1], T R Welberry[1], M J Gutmann[3] and R O Piltz[4]

[1] Research School of Chemistry, The Australian National University, Canberra, ACT 0200, Australia
[2] Department of Physics, The Australian National University, Canberra, ACT 0200, Australia
[3] ISIS Facility, Rutherford Appleton Laboratory, Chilton, Didcot, Oxon, UK
[4] Bragg Institute, Australian Science and Technology Organisation, Lucas Heights, NSW 2234, Australia

E-mail: goossens@rsc.anu.edu.au

Received 10 September 2008, in final form 17 October 2008
Published 25 February 2009
Online at stacks.iop.org/JPhysCM/21/124204

Abstract

Neutron diffuse scattering is used to explore the short-range order (SRO) in deuterated *para*-terphenyl, $C_{18}D_{14}$. The crystal shows SRO because the central of the three phenyl groups of each molecule can twist positively or negatively and these twists are correlated over the local scale. The presence of incipient Bragg peaks at $(\frac{1}{2}\ \frac{1}{2}\ 0)$ at 200 K shows that these flips are negatively correlated along the **a** direction (nearest neighbour correlation coefficient of ∼–0.3) and **b** direction (nearest neighbour correlation coefficient of ∼−0.87) and appear essentially uncorrelated along **c**. Diffuse peak anisotropy indicates that the range of the correlations along **b** is found to be ∼3 times that along **a**. These correlations persist, although weaker, at room temperature.

A Monte Carlo simulation was used to impose a correlation structure on the population of central ring twists that was deduced from Bragg scattering. By then allowing displacive relaxation of the structure, the observed diffuse scattering was well reproduced.

Modelling the displacive motions of molecules showed that the positions of nearest **ab**-plane neighbour molecules are strongly positively correlated, particularly for motions approximately parallel to **a**, while the displacive correlations are weaker between molecules stacked along **c**. The apparent contradiction that the displacements are most strongly correlated along **a** while the occupancies are most strongly correlated along **b** is explained in terms of the connectivity of molecular interactions.

(Some figures in this article are in colour only in the electronic version)

1. Introduction

Diffuse scattering, whether of x-rays or neutrons, from organic molecular crystals can provide a wealth of information, not only on the short-range order (SRO) in the material, but in some cases on molecular dynamics in the solid state [1–3]. The molecular dynamics information is limited to cases in which the fitting of the diffuse scattering allows intramolecular potentials to be reliably determined, and when the dynamics resulting from these potentials allow a relatively simple interpretation. The result is a real-space picture of molecular modes in the crystal, very unlike, for example, plotting a phonon dispersion curve based on inelastic neutron scattering results. That is not to say that diffuse scattering cannot be used to explore phonons, as was shown in [3].

A family of materials whose molecular dynamics and SRO have been much-studied are the polyphenyls, many of which exhibit fascinating SRO, from the incommensurate ordering in biphenyl [4] through to the many structural phase transitions and forms of ordering present in the more complex variants [5–8].

In this paper, neutron diffuse scattering from a single crystal of deuterated *para*-terphenyl (d-ptp) is used to examine

[5] Author to whom any correspondence should be addressed.

models of the SRO in *para*-terphenyl. Through direct observation of the diffraction features resulting from the SRO, insight into the intermolecular interactions can be gained. The analysis acts as a test of existing models of the material, and in addition allows investigation of the population of molecular conformations that gives rise to the average structure revealed by Bragg scattering.

Para-terphenyl undergoes a structural phase transition at 193 K. The high temperature phase has lattice parameters $a = 8.106(4)$ Å, $b = 5.613(2)$ Å, $c = 13.613(6)$ Å and $\beta = 92.04(4)^\circ$ at room temperature, with space group $P2_1/a$ [9]. The low temperature structure comes from a doubling along **a** and **b**; it is triclinic, space group $P1$, with a pseudo-monoclinic cell [10, 11]. The central ring of each molecule lies at an angle to a plane containing the outer rings. This is because of competition between inter-ring H–H contacts between *ortho*-hydrogens, which try to force the adjacent rings to be non-coplanar, and the conjugation of the π orbitals on the phenyl rings (see figure 1), which prefer a coplanar arrangement for all rings. Within the crystal frame of reference, this results in two possible 'motifs': (1) molecules in which the centre ring is twisted in one sense, and (2) those in which it is twisted oppositely. Below T_C, these motifs order in a long-ranged fashion, alternating along **a** and **b**, giving the $P1$ cell which has a doubling along **a** and **b** relative to the high temperature $P2_1/a$ cell. Above T_C, the range of this ordering becomes finite so that the average structure unit cell is the $P2_1/a$ cell, but the existence of the two senses of twisting is apparent in the atomic displacement parameters for the centre ring as compared to those for the outer rings.

Earlier work modelled the scattering at the incipient superlattice points using a Lorentzian function

$$I(\mathbf{q}) = \frac{AT}{\xi^{-2}(1 + \xi_h^2 q_h^2 + \xi_k^2 q_k^2 + \xi_l^2 q_l^2)} \qquad (1)$$

where A is a constant, T is temperature, ξ measures the correlation length of the fluctuations and the remaining three terms give the widths in three directions which are approximately orthogonal [12]. This function can be directly fitted to the observed incipient superlattice peak; but while such a fit may deliver the correlation structure of the SRO, it says little about the molecules which are being correlated. Recently developed methods to analyse diffuse scattering combine the ability to reveal the correlation structure as shown in the earlier diffuse scattering study [12] with the ability to quantitatively explore the shape of the correlated molecules, similar to the analysis of anisotropic thermal parameters from Bragg scattering, but in greater detail. Work presented in [12] concluded that 'The correlations in *para*-terphenyl are anisotropic, being ratios ξ_1:ξ_2:$\xi_3 \simeq$ 2:6.5:1 near T_C' (with ξ_2 (ξ_k) being given as 344 Å, or about 60|**b**| at $T = T_C + 4$ K). Data used in the current work were measured at 200 K, but on deuterated *para*-terphenyl, for which $T_C \simeq 178$ K [13] (hence $T = T_C + 22$ K).

The distribution of the torsional angle on the central phenyl ring as derived from Bragg studies is presented in the literature [14, 15]; because of the double-well potential

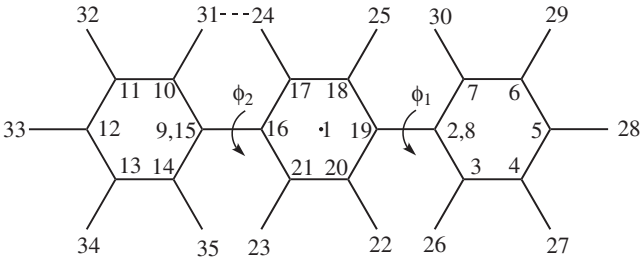

Figure 1. Schematic diagram of the *para*-terphenyl molecule, with internal twist angles ϕ_1 and ϕ_2 noted. Atom numbering accords with that used in the z-matrix (see below). Atoms 1, 2 and 9 are 'dummy' atoms used to define the internal molecular coordinates. An example of the H–H *intra*molecular contacts which prefer a non-coplanar configuration of the rings is noted as a dashed line. Note that in practice the model uses only a single rotation angle, ϕ, which gives the angle of the central ring to the plane of the outer two.

that results from the intramolecular interactions, this is a two-peaked distribution. The key parameters are the offset of the histogram maxima from zero ($\sim$13.2°), the widths of the peaks and, related to this, the histogram value at zero twist, which gives the barrier height for transitions between the two wells of the potential. The distribution derived from analysis of the average structure has been compared to results derived from modelling of the molecular dynamics (MD) [16]. In that work some account of intermolecular correlation was taken [16] but this was limited by the small size of the detailed MD simulation—4 × 4 × 2 unit cells. By using a large model, 32 × 32 × 32 unit cells, the population of local configurations that gives rise to the average can be modelled. Such a size was chosen for the present work as a compromise between the apparent range of correlations and speed of calculation. Such a model not only tests the distribution of torsion angles, but also allows modelling of the correlation structure amongst the molecular displacements.

2. Experimental details

A single crystal of d-ptp was grown from the melt using a Bridgman approach. A polycrystalline ingot of d-ptp inside a glass tube with an extended tip was suspended from a metal chain in a vertical tube furnace. The furnace was held at 230 °C for 2 h to ensure that all the material was molten, then the ampoule was lowered at a rate of 0.5 mm h^{-1} for 14 days. As the ampoule moved down, the line of solidification moved through the tip, such that when it reached the body of the ampoule, a single crystal orientation prevailed. The resulting ingot was not a single crystal but contained a large single crystal amidst a number of smaller ones. *Para*-terphenyl is extremely soft, and so separating the desired crystal required considerable care. The final crystal used in the experiment was approximately 8 × 4 × 1 mm^3.

Data were collected on the SXD single crystal diffractometer at the ISIS neutron source using a similar approach to that detailed previously [3]. Three-dimensional distributions of scattering were collected at room temperature (295 ± 3 K), 200 ± 5 K and 70 ± 5 K. That is to say, the crystal was mounted

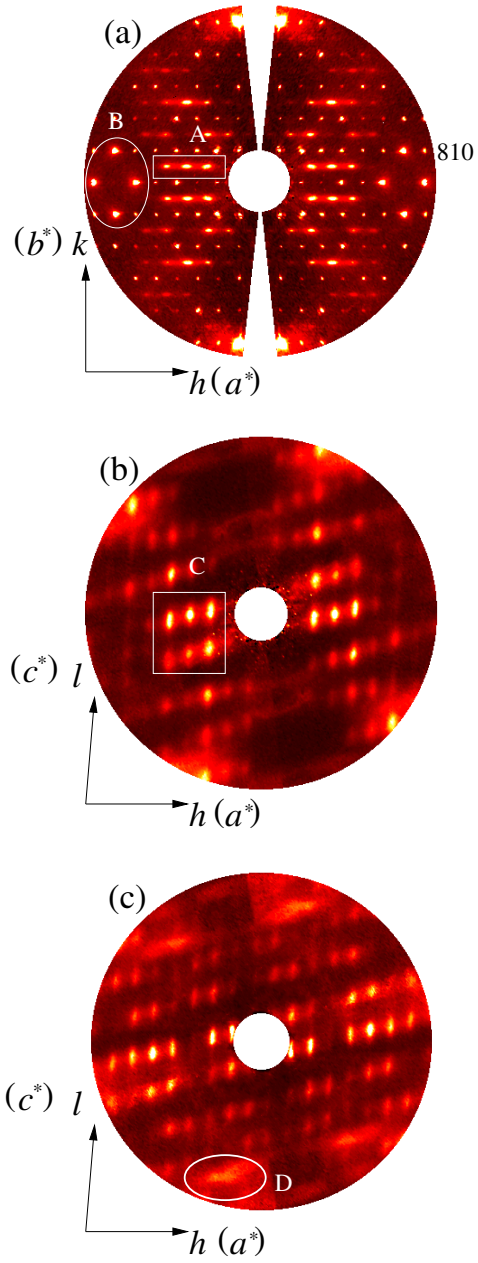

Figure 2. Diffuse scattering from d-ptp measured on SXD at 200 K. (a) The $hk0$ plane. The 8 1 0 reciprocal lattice point is noted to indicate scale: all planes are to the same scale. (b) $h0.5l$. (c) $h1.5l$. Superlattice peaks are boxed on (a) and (b) (regions A and C), while examples of regions of thermal diffuse scattering are noted by ellipses (B, D).

in a closed cycle helium refrigerator with the sample ab plane in the equatorial plane of the instrument. At 200 K, diffracted neutron intensity was collected for two hours at each of five sample angle (ω) settings, with the sample rotated around a vertical axis (keeping the ab plane horizontal) by 20° between settings, such that over 100° was swept out. The sample was then tilted by 45° and four more settings, again at 20° increments, were completed. At 70 K and room temperature, only the initial set of five sample settings were collected.

Data were processed using the SXD2001 program [17], which allowed symmetry to be applied to the data which, when combined with the large solid angle of SXD, allowed the planes of data, such as those shown in figure 2, to be assembled.

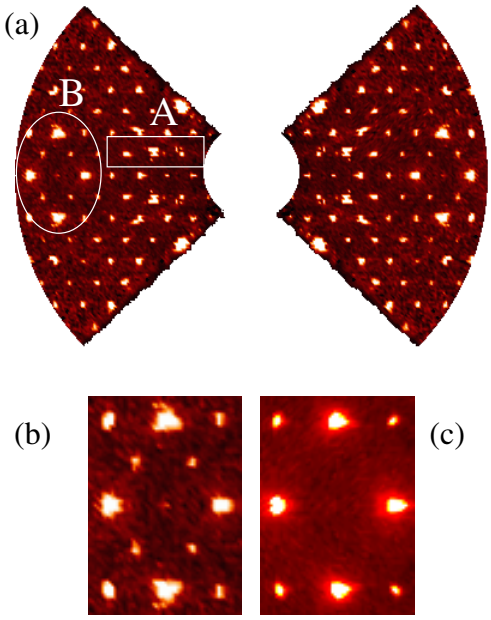

Figure 3. (a) The $hk0$ plane of reciprocal space as measured at 70 K on SXD. (b) A close up of the circled area, region B, in (a). (c) The same region measured at 200 K. Despite the poorer statistics of the 70 K data, the superlattice Bragg peaks are quite apparent in (b) compared to (c).

3. The data

Initial examination of the data allows a range of conclusions to be drawn.

Figure 2 shows several planes of reciprocal space in false-colour maps, where black indicates zero intensity and white maximum. These data were measured at 200 K. Immediately apparent are the large oval regions of diffuse scattering at the $(hkl) + (\pm\frac{1}{2}\ \pm\frac{1}{2}\ 0)$ Bragg positions in the $hk0$ cut (figure 2(a), region A). These are incipient Bragg peaks and below T_C they sharpen into real Bragg peaks (see figure 3(b)). These hold information about the correlations between the twists on adjacent molecules, which will also be referred to as 'occupancy correlations'. The strong anisotropy indicates that the correlations are much stronger in the **b** direction than in the **a** direction. In terms of nearest neighbour correlations, the **b** direction correlations are approximately three times stronger, though the ratio $|\mathbf{b}|:|\mathbf{a}|$ is only 5.613:8.106. The lack of correlation along **c** (shown in figures 2(b) and (c), particularly region C) is not unexpected, as it is the outer phenyl groups that form contacts from molecule to molecule in this direction, so molecules stacked along **c** are essentially insulated from the occupancies of their neighbours (figure 4(a)). Also apparent are the large regions of thermal diffuse scattering (examples are noted in regions B and D). These regions are not strongly structured, suggesting that the molecular motions are correlated relatively isotropically in this plane.

The $hk0$ cut at 70 K is shown in figure 3(a). The data are not as comprehensive as those in figure 2(a), and the

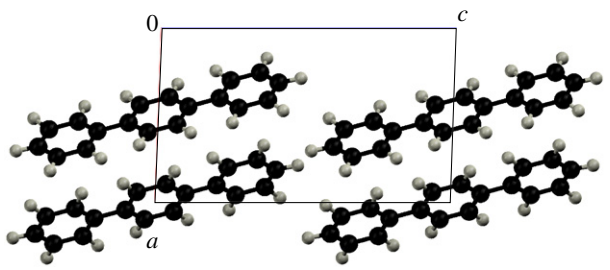

Figure 4. A unit cell of d-*para*-terphenyl with the molecule treated as 'flat', viewed down the b^* axis.

statistics are poorer, but they do show that, within the limits of instrumental resolution, crystal size and mosaic, the diffuse peaks at ($\frac{1}{2}$ $\frac{1}{2}$ 0)-type positions (again boxed) have sharpened into real Bragg peaks. The change is perhaps most apparent in a close up of the circled area. Figure 3(b) shows the circled area from figure 3(a) while figure 3(c) shows the corresponding region at 200 K (taken from figure 2(a)).

At 70 K, the three diffuse ovals boxed in figure 2(a) become a row of Bragg peaks (figure 3(a)). As the peak width gives a measure of the sizes of the regions over which the molecular twists are correlated, then by deconvoluting the intrinsic Bragg widths from the diffuse peaks, the sizes and shapes of the diffuse ovals at 200 K can be used to measure the length scale of the SRO. Correlation lengths were deduced by fitting the line profiles with a convolution of a Gaussian (whose width was fixed by the widths of neighbouring Bragg peaks and represented instrumental width and factors such as sample mosaic) with a Lorentzian whose width came from the finite range of the correlations. Such fits gave correlation lengths (at 200 K) along **a** and **b** of $\xi_a \sim 55$ Å ($\sim 7|\mathbf{a}|$) and $\xi_b \sim 160$ Å ($\sim 29|\mathbf{b}|$), a ratio of $\xi_b/\xi_a \sim 3$. Given that these data were measured at $T_C + 22$ K, these results accord quite well with those given in table 1 of [12]. The ratio also accords well with previous results for ξ_a:ξ_b of 1:2.65 [12] and 3:8 [13].

At room temperature, there is still structure in the scattering, though it is weaker; data suggest correlation lengths of ∼30 Å along **a** (∼4|**a**|) and ∼60 Å along **b** (∼11|**b**|), which are still substantial, but far shorter than at 200 K.

The data measured at 200 K are by far the best in terms of counting statistics, and so detailed modelling is centred on these data. Data suggest that the SRO at room temperature (RT) is not different qualitatively from that at 200 K, merely less pronounced.

4. The modelling

In order to test the model of molecular conformation and SRO in *para*-terphenyl established in the literature [12, 16], a model was constructed in which the histogram of central ring torsion angles was taken from the literature [14] and a correlation structure was then induced in this population using a simple Monte Carlo (MC) algorithm. By using an MC step in which the model crystal's energy was compared before and after exchanging the torsion angles on two randomly chosen molecules, the overall distribution of torsion angles was maintained, ensuring that the average structure was maintained.

The torsion angles on the centre rings of the molecules relative to the plane of the outer two rings were treated as an array of real numbers onto which a desired correlation structure was imprinted by what is referred to herein as an 'occupancy simulation'. The simulation approach used was a Monte Carlo algorithm, in which the 'energy' of the ith molecule was given by

$$E_i = \sum_j w_{ij}\phi_i\phi_j \qquad (2)$$

where the ith molecule has N interacting neighbours indexed by j, ϕ_i is the centre ring torsion angle on molecule i and w_{ij} is a force constant for the interaction between angles on the correlated molecules. Some of these neighbours are nearest neighbours in the **a** direction, so for these $w_{ij} = w_a$ and similarly for other classes of neighbours. The model crystal was allowed to equilibrate through Monte Carlo simulation, and the correlation structure then calculated. The w_{ij} were then automatically adjusted to better give the desired correlations, and the process iterated until the desired correlations existed in the model. Equilibration proceeded as follows: two molecules were selected at random from the array, and their energies calculated according to equation (2). The ϕ values on the two molecules were then swapped, and the energy calculation repeated. If the new configuration was of lower energy, it was kept, otherwise it was rejected or accepted with a probability depending on the temperature of the system [18]. After many such steps, the system had reached equilibrium. Its correlation structure was then calculated, the w_{ij} adjusted by comparing the observed with the desired correlation structure, and the simulation repeated until the desired correlation structure was obtained.

The array of correlated angles resulting from the occupancy simulation was then imprinted onto a $32 \times 32 \times 32$ array of unit cells. The imprinting was done by describing the molecule using a z-matrix (table 1). A z-matrix defines each atom in the molecule in terms of those defined previously. By changing a single variable on a single atom (in this case the torsion angle on atom 17) the positions of all dependent atoms could be automatically updated. The molecule as a whole was then positioned into the model crystal by positioning the origin atom using a three-vector, **x** and by orienting the molecule's first bond within the crystal frame of reference (using a quaternion, **q** [19]). Any internal degrees of freedom that are allowed to vary, for example rotations around C–C single bonds, are stored in a vector, **i**. In this case there was only a single element in **i**, the angle ϕ of the central phenyl group to the plane containing the outer rings.

Once the model crystal was constructed, the diffuse diffraction pattern of the array of molecules was then calculated. In a further elaboration, the array was relaxed displacively such that the molecules could interact, subject to the torsional angles being fixed by the occupancy simulation discussed above. Thus they could displace from their average positions, and reorient as rigid units within the crystal.

In this 'displacive' simulation, a molecule was considered to interact with neighbouring molecules via contact vectors that

Table 1. The z-matrix for d-*para*-terphenyl as used in the analysis. Atoms with labels prefixed 'x' are 'dummy' atoms used to aid in defining the local coordinate system and internal degrees of freedom. The starred (*) value is replaced by a dihedral angle taken from the bimodal distribution. All other values are fixed during the modelling. Numbers in the first column correspond to those in figure 1.

	Label	l	Distance from l (Å)	m	Angle with lm (deg)	n	Dihedral angle with lmn (deg)
1	x1	—	—	—	—	—	—
2	C4	1	2.912	—	—	—	—
3	C5	2	1.406	1	120.510	—	—
4	C6	3	1.395	2	120.251	1	179.771
5	C7	4	1.387	3	120.678	2	−1.240
6	C8	5	1.384	4	119.710	3	1.561
7	C9	6	1.394	5	120.468	4	−1.155
8	x2	7	1.409	6	120.519	5	0.432
9	C4B	8	5.825	7	121.127	6	−179.368
10	C5B	9	1.406	8	120.510	7	−0.750
11	C6B	10	1.395	9	120.251	8	−179.771
12	C7B	11	1.387	10	120.677	9	1.240
13	C8B	12	1.384	11	119.710	10	−1.561
14	C9B	13	1.394	12	120.468	11	1.155
15	x2B	14	1.409	13	120.519	12	−0.432
16	C2B	15	1.329	14	121.037	13	179.518
17	C1B	16	1.407	15	121.135	14	−180.000*
18	C3B	17	1.393	16	121.658	15	−179.878
19	C2	18	1.406	17	120.534	16	−0.732
20	C1	19	1.407	18	117.804	17	0.700
21	C3	20	1.393	19	121.658	18	−0.713
22	D1	20	1.107	21	118.327	19	−176.663
23	D2	21	1.061	20	118.909	22	5.629
24	D1B	17	1.107	18	118.327	16	176.662
25	D2B	18	1.061	19	120.538	17	−178.415
26	D3	3	1.064	4	121.032	2	−171.714
27	D4	4	1.056	5	122.918	3	−178.101
28	D5	5	1.042	6	118.647	4	176.696
29	D6	6	1.127	7	118.434	5	170.882
30	D7	7	1.066	8	122.600	6	174.386
31	D3B	10	1.064	11	121.033	9	171.714
32	D4B	11	1.056	12	122.918	10	178.101
33	D5B	12	1.041	13	118.647	11	−176.696
34	D6B	13	1.127	14	118.434	12	−170.882
35	D7B	14	1.066	15	122.600	13	−174.386

act as springs and whose energy is given by Hooke's law.

$$E_i = \sum_{\text{cv}} F_{\text{cv}} (d_{\text{cv}} - d_{\text{cv0}})^2 \qquad (3)$$

where d_{cv} is the instantaneous length of the given contact vector, d_{cv0} is its 'equilibrium length' and F_{cv} is its associated force constant. The model uses a subset of the nearest neighbour atom–atom contact vectors. By doing so, the interactions must be considered as 'effective' interactions only, and while the associated F_{cv} may be indicative of the relative strengths of the interactions in different directions, they should primarily be considered as a mechanism for inducing a correlation structure into the displacements.

In the displacive simulation, a single molecule was selected at random and its energy calculated through equation (3). The molecule's configuration was then randomly altered, which is to say its position and orientation were modified, and its energy recalculated. The new configuration was accepted or rejected according to a Metropolis-like algorithm [18]. After thousands of such steps per molecule, the contact vectors induced a correlation structure into the displacements and orientations of the molecules. Rather than fixing the temperature of the simulation, the F_{cv} were dynamically scaled such that the average atomic displacements of the atoms in the molecules were similar to that obtained in single crystal studies.

Figure 5 shows the $hk0$ plane calculated from a model with the torsional angles showing correlations of −0.87 in the $\hat{\mathbf{b}}$ direction, −0.3 in $\hat{\mathbf{a}}$ and 0 in $\hat{\mathbf{c}}$. *Uncorrelated* whole-molecule displacement variations have been added. As can be seen immediately, the key occupancy features have been reproduced (see for example box A), while the large diffuse peaks of displacive origin noted in figure 2 (B and D) have not; but there is broad diffuse intensity in the correct regions of reciprocal space (see box B) which correlation of the molecular displacements is expected to modulate. Indeed, the discrepancy shows that it is *essential* to correlate these displacements and orientations *as well as* the torsional twists.

Figure 7 shows the diffraction patterns of the same cuts as in figure 2 calculated from a model with the F_{cv} from equation (3) adjusted to best match the observed displacive scattering. The model well reproduces the data. While there are 49 symmetry inequivalent contact vectors used to connect molecules, they have been grouped into only six

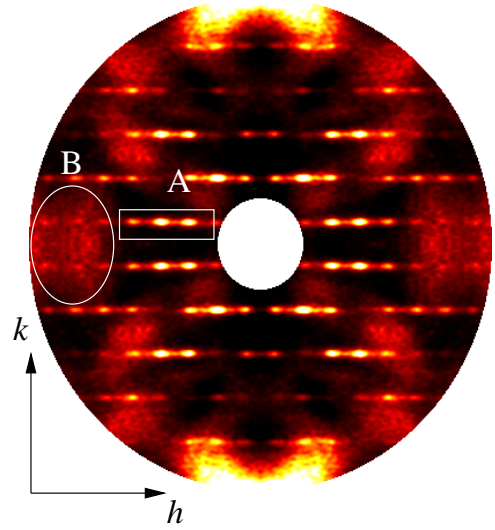

Figure 5. The $hk0$ plane of reciprocal space of d-*para*-terphenyl, calculated from a model in which the population of torsional angles on the central ring is taken from [14, 16] and then values on neighbours are correlated such that nearest neighbour correlation in the $\hat{\mathbf{a}}$ direction is -0.3, in the $\hat{\mathbf{b}}$ direction -0.87 and 0 in $\hat{\mathbf{c}}$. Molecules have been given uncorrelated overall displacements.

classes depending on the direction of propagation and which types of neighbours the vectors connect. Hence, this model uses two numbers to parametrize the correlation in twists of angles and six for the displacive part to well reproduce a large three-dimensional (3D) data set from which these three slices have been focused on as being most useful. Further, while there are six contact vector classes, only two differing values of force constant were used—meaning that only four parameters were used to model approximately 1×10^5 pixels.

Examples of the six contact vector classes are shown in figure 6.

Broadly, they can be described as follows:

(i) Class 1 vectors connect molecules adjacent along the molecular long axes (approximately the $\pm\hat{\mathbf{c}}$ directions).
(ii) Class 2 vectors connect molecules adjacent along the $\pm\hat{\mathbf{b}}$ directions.
(iii) Class 3 vectors connect molecules adjacent along the $\pm\hat{\mathbf{c}}$ directions.
(iv) Class 4 vectors connect molecules adjacent along directions approximately parallel to $\mathbf{a} \pm \mathbf{b}$, with the vector itself pointing in approximately these directions.
(v) Class 5 vectors connect molecules adjacent along a direction approximately parallel to $\mathbf{a} \pm \mathbf{b}$, with the vector itself pointing in approximately the $\pm\hat{\mathbf{a}}$ directions.
(vi) Class 6 vectors connect molecules adjacent along a direction approximately parallel to $\mathbf{a} \pm \mathbf{b}$, with the vector itself pointing in directions intermediate between classes 4 and 5.

Relative to $k_B T$, classes 1–3 are given a value of $F_{cv} = 3.1 \pm 0.2$ and classes 4–6 a value of $F_{cv} = 0.5 \pm 0.1$. However, it must be noted that vectors which propagate laterally relative to the long axis of the molecule are much greater in number

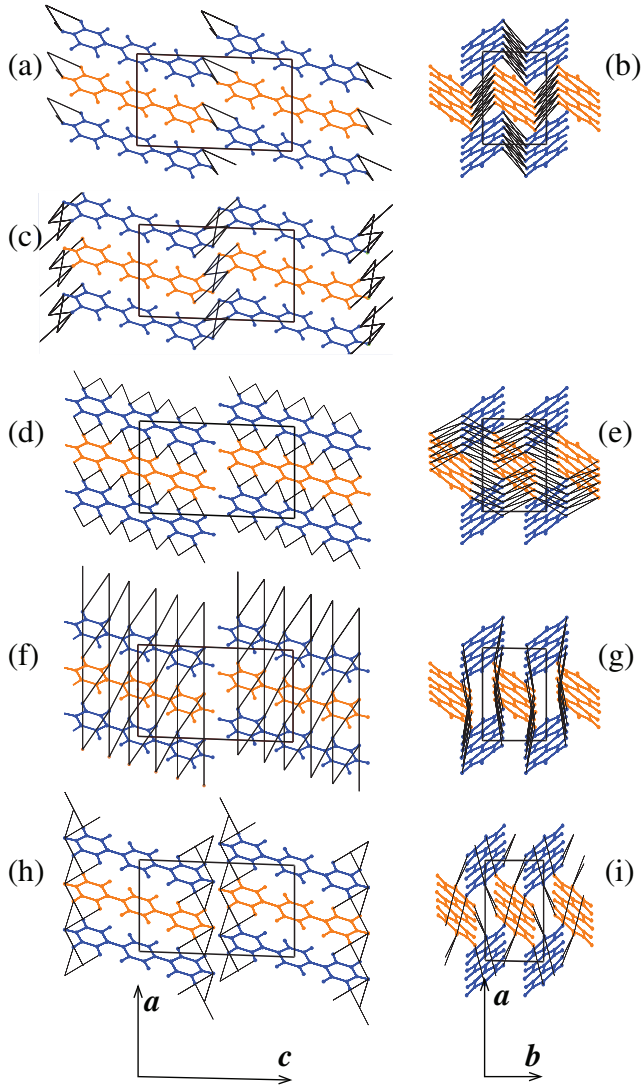

Figure 6. Illustration of the sets of contact vectors used. (a) Class 1. (b) Class 2. (c) Class 3. (d) and (e) Class 4. (f) and (g) Class 5. (h) and (i) Class 6. The different shadings of molecules indicate the two molecules in the unit cell.

due to the molecular packing, and this tends to mean the F_{cv} values of the individual vectors are lower.

All the regions A, B, C and D are well reproduced, with almost all the details of the observations present in the calculations. The SXD data show some instrumental effects (best seen in the distorted Bragg spots shown in figure 3).

5. Analysing the model

Once this model was established, it could be explored. The first point to note is that there was no 'size-effect' [20] needed to model the data. Size-effect induces asymmetry in diffuse peaks, something which is not apparent in figure 2. The lack of size-effect indicates that molecules do not push apart or pull together significantly depending on the torsional twist. The lack of size-effect makes sense for molecules stacked along **c** because in this direction only the outer phenyl rings are in contact. It is more surprising in the **ab** planes. However, since

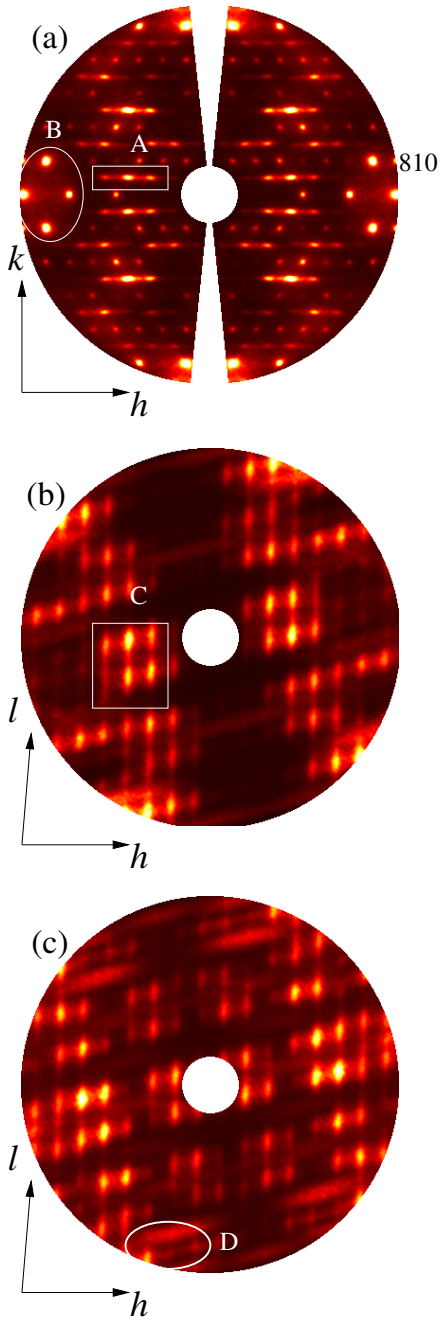

Figure 7. Diffraction patterns calculated from a model in which the population of torsional angles on the central ring is taken from [14, 16] and then values on neighbours are correlated such that nearest neighbour correlation in the $\hat{\mathbf{a}}$ direction is −0.3, in the $\hat{\mathbf{b}}$ direction −0.87 and 0 in the $\hat{\mathbf{c}}$ direction. Overall molecular displacements and orientations have been correlated via equation (3) to make the displacive features qualitatively similar to those in the observations.

a majority of the interactions in the system involve the outer pair of phenyl rings—which show no occupancy structure—they will serve to define the intermolecular distances in a way which is largely independent of the twists on the contacting molecules. The interactions between inner rings will be responsible for propagating the correlations on the twist angles.

5.1. Occupancy correlation structure

The occupancy structure, which is to say the structure in the distribution of middle-phenyl-ring twists on the molecules, which gave the best fit to the observed data was produced with nearest neighbour correlations of −0.87 for neighbours adjacent along **b** and −0.3 for neighbours adjacent along **a**, as suggested by the anisotropy of the diffuse peaks in box A in figure 2. The **b** axis correlation is −0.87 rather than $3 \times -0.3 = -0.9$ because the width of the histogram of angles used [14] limited the maximum value of correlation obtainable. Direct correlations with more distant neighbours did not need to be specified to model these data—only nearest neighbour correlations were specified in the MC, with more distant neighbour correlations arising naturally as a result. Comparison of figure 2 to figure 7 shows that the extent and modulation in $\hat{\mathbf{c}}^*$ (l) of the same spots (box C in the figures) is also well reproduced. Also well reproduced are the systematic variations in the intensities of the diffuse peaks in figures 2(c) and 7(c).

5.2. Displacive correlation structure

The correlation structure of the displacements is one of the results which the analysis presented here can obtain and is lacking in previous studies [12, 14, 16]. One way to present this data is in the form of correlation vector diagrams (figure 8).

These diagrams show the correlations between the displacements of molecular origins for adjacent molecules, connected by a given class of contact vector, as a function of the direction of the displacements. In practice, each molecule in the crystal is visited and the component of its displacement from the average position along a given direction is found. The same calculation is performed for the molecules which it contacts. The result is two columns of numbers whose correlation is calculated before moving on to the next displacement direction. The end result is a polar plot, where the magnitude is the correlation coefficient and the angle is the angle the molecular displacement component makes to a reference direction. Such a plot shows in which directions molecular motions are strongly correlated and in which directions they are weakly correlated.

Figure 8 shows that displacement correlations are strong between displacement components lying in the **ab** plane for molecules which are neighbours in the **ab** plane (connected by classes 2 and 6, for example). Class 1 contact vectors connect molecules which are stacked along the molecular long axes, and the correlations here are substantially weaker, even for displacements along the lengths of the molecules, which might be expected to be relatively strong. Such results indicate that the structure is to a large degree describable as a series of **ab** sheets stacked up along **c** and interacting only (relatively) weakly. This is an example of the dangers inherent in directly interpreting the force constants—the force constants acting along **c** are amongst the strongest, but the relative scarcity of these interactions means the correlations remain weak.

Class 2 contacts connect molecules adjacent in **b**, but figure 6 shows why it is plausible that it is the **a** components of the displacements which are most strongly correlated—it is

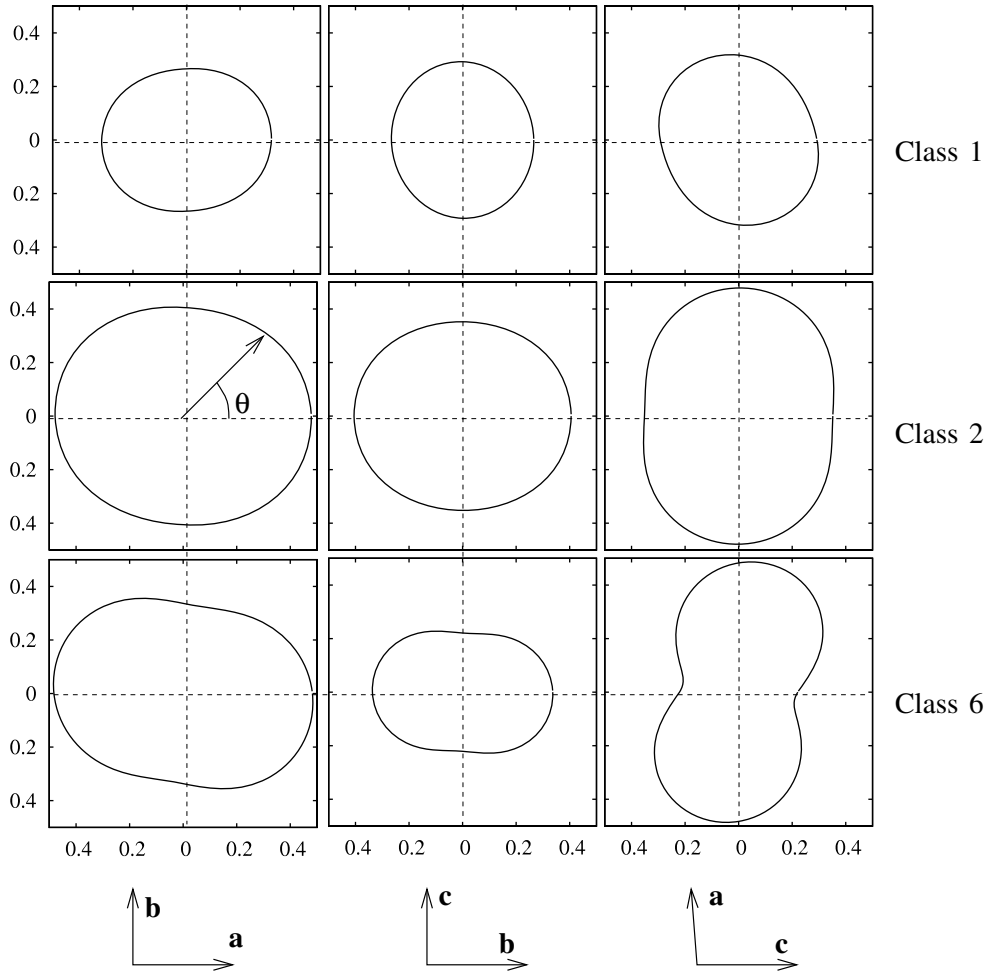

Figure 8. Some aspects of the correlation structure of molecular displacements in *para*-terphenyl at 200 K. The length of the radial vector gives the magnitude of the correlations between components of the displacements at an angle of θ to the horizontal axis, as noted at the bottom.

because the contacts themselves are far from parallel to **b**, and act in concert with other contacts such as those from class 5 (figure 6(g)) which are predominantly directed along **a**.

It is possible to examine correlations between the variables that describe molecules, denoted **x**, **q** and **i** in section 4. It is found that *within* a molecule the quaternion and the internal twist angle are significantly correlated. Interpretation is not simple because **q** is normalized, but the correlation between ϕ (see figure 1) and q_1, the first component of **q**, is $r \sim 0.7$. Such a correlation makes sense because when the centre ring twists some contacts are deformed and then the molecule can reach a compromise between satisfying the centre ring and the outer rings by changing its overall attitude.

No other correlations between variables within a given molecule are significant.

Considering molecules connected by contact vectors of class 1, it is found that, as anticipated, the ϕ angles are essentially uncorrelated, and the only correlations greater than 0.2 are between x_1 and x_2 ($r \sim 0.29$), y_1 and y_2 ($r \sim 0.26$) and z_1 and z_2 ($r \sim 0.26$) (where for example x_1 is the x-coordinate of one molecule and x_2 that of its neighbour). In other words, the molecules are weakly transferring their global motions to their neighbours.

Considering molecules connected by contact vectors of class 2, results are more striking. The correlations noted above are present but much stronger between x_1 and x_2 ($r \sim 0.47$), y_1 and y_2 ($r \sim 0.41$) and z_1 and z_2 ($r \sim 0.33$); but there are also strong correlations between ϕ angles on contacting molecules ($r \sim -0.87$) (see figure 9) and between the ϕ on one molecule and the quaternion **q** of the neighbour ($r \sim -0.57$ between ϕ_1 and q_{12} where q_{i2} is the ith component of the quaternion on the neighbouring molecule). Similarly, the quaternions of contacting molecules are correlated. This indicates that the orientation of one molecule is influencing that of its neighbour, which must be happening because of attempts by the displacive structure to accommodate the occupancy structure imprinted onto the model crystal. One conclusion to be drawn from this is that it may be possible to find an arrangement of contact vectors out of which the correlation structure of the twists (the occupancy correlations structure) arises naturally, during the displacive simulation rather than being imposed by the occupancy simulation and then fixed. Such a model is a further aim of this study.

Considering molecules connected by contact vectors of class 6, there is little correlation between ϕ angles and quaternions, and the case is not unlike that for class 1 except

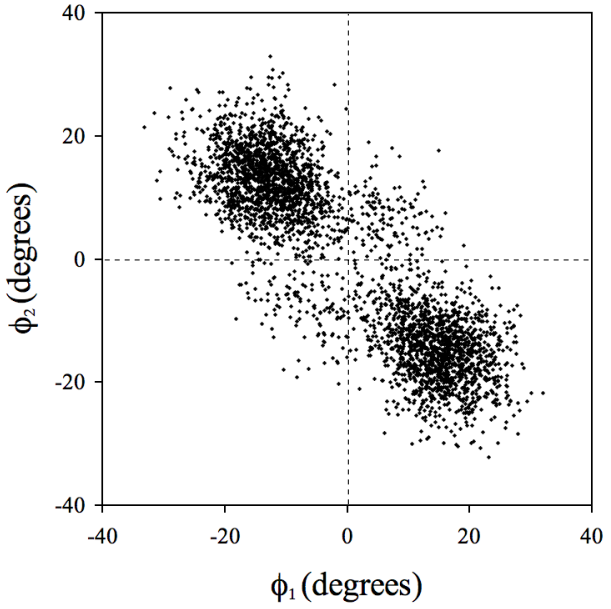

Figure 9. Scatter plot of the central ring torsion angle on one molecule (ϕ_2) against that on a neighbour which it is contacting via class 2 contact vectors (ϕ_1). The bimodal distribution and substantial negative correlation are apparent.

the correlations are stronger between x and y coordinates and weaker between z coordinates, which makes sense as these contacts do little to constrain motions in z. The significant correlations are between x_1 and x_2 ($r \sim 0.48$), y_1 and y_2 ($r \sim 0.33$) and z_1 and z_2 ($r \sim 0.21$).

Hence, the final picture is one in which the occupancy correlations are strongest between neighbours adjacent along **b**, because such neighbours are in close proximity and the twist on one molecule can most easily influence that on the next (via interactions of class 2), whereas the displacive correlations are strongest for displacements in the **a** direction (although also very strong for displacement components anywhere in the **ab** plane) between neighbours which are either nearest neighbours along **b** or along **a** $\pm$ **b**-type directions, Nearest neighbours along **a** are not close enough to contact directly and can only interact indirectly via the other sorts of neighbours, and this explains the weak occupancy correlations along **a**.

6. Conclusions

At 200 K, the twists on the central phenyl ring of d-*para*-terphenyl show nearest neighbour correlations of approximately -0.3 in the $\hat{\mathbf{a}}$ direction, -0.87 in the $\hat{\mathbf{b}}$ direction and 0 in $\hat{\mathbf{c}}$. These correlations accord with earlier results [12, 13], and suggest that the histogram of molecular twists presented in [14–16, 21, 22] is reasonable. That work supposed a double-well potential on the torsional twist with a barrier height of approximately 1.5 kcal mol^{-1} at 180 K (1.1 kcal mol^{-1} at 300 K [16]) and minima separation of 26°.

Other similar systems show similar barrier heights, although estimates vary and a single figure for each system (and therefore an overall trend) is difficult to arrive at, especially given the likely temperature dependence. Suggested barrier heights for biphenyl include 1.4 kcal mol^{-1} [23] and 2.2 kcal mol^{-1} [24]. Quoted figures for quaterphenyl include 1.0 kcal mol^{-1} [25].

New insights come when modelling the displacive scattering. It has been shown that the strongest nearest neighbour displacive correlations have a value of approximately 0.5, and are between $\hat{\mathbf{a}}$-direction displacements of molecules adjacent in the $\hat{\mathbf{b}}$ direction and in **a** $\pm$ **b**-type directions. No size-effect parameters were needed to model the data well, but that is not to say that occupancy (torsional twist) and overall molecular confirmation and position are decoupled. In fact it was shown that the position of the molecular origin is essentially independent of the torsional twist angle, ϕ, but the molecular *orientation* around that origin is not. The quaternions compensate for the twist on the central ring, which is to say that the overall orientation of the molecule is correlated with the twist on its central ring. This then acts to stretch and compress contact vectors, correlating the twists on the central rings of molecules adjacent in the **ab** plane. The lack of contact vectors acting directly between $\hat{\mathbf{a}}$-direction neighbours means that the effects of the twists have to be transmitted indirectly and this explains the weak occupancy correlations in this direction.

Acknowledgments

The support of the Australian Research Council, the Australian Partnership for Advanced Computing and the Access to Major Research Facilities Programme are gratefully acknowledged. DJG gratefully acknowledges the support of the Australian Institute of Nuclear Science and Engineering (AINSE), both through an AINSE Fellowship and through grant AINGRA05199.

References

[1] Welberry T R, Goossens D J, Edwards A J and David W I F 2001 *Acta Crystallogr.* A **57** 101–9
[2] Welberry T R, Goossens D J, Haeffner D R, Lee P L and Almer J 2003 *J. Synchrotron Radiat.* **10** 284–6
[3] Welberry T R, Goossens D J, David W I F, Gutmann M J, Bull M J and Heerdegen A P 2003 *J. Appl. Crystallogr.* **36** 1440–7
[4] Cailleau H, Moussa F and Mons J 1979 *Solid State Commun.* **31** 521–4
[5] Délugeard Y, Desuche J and Baudour J-L 1976 *Acta Crystallogr.* B **32** 702–56
[6] Saito K, Yamamura Y, Saitoh H, Matsuyama H, Kikuchi K and Ikemoto I 1994 *Solid State Commun.* **92** 495–9
[7] Baudour J-L 1991 *Acta Crystallogr.* B **47** 935–49
[8] Baudour J-L, Délugeard Y and Rivet P 1978 *Acta Crystallogr.* B **34** 625–8
[9] Rietveld H M, Maslen E N and Clews C J B 1970 *Acta Crystallogr.* B **26** 693–706
[10] Baudour P J-L, Délugeard Y and Cailleau H 1976 *Acta Crystallogr.* B **32** 150–4
[11] Baudour P J-L and Charbonneau G-P 1974 *Acta Crystallogr.* B **30** 1379
[12] Welberry T R and Mair S L 1987 *J. Phys. C: Solid State Phys.* **20** 4773–81
[13] Lechner R E, Toudic B and Cailleau H 1984 *J. Phys. C: Solid State Phys.* **17** 405–20

[14] Baudour P J-L, Cailleau H and Yelon W B 1977 *Acta Crystallogr.* B **33** 1773–80
[15] Baudour P J-L 1991 *Acta Crystallogr.* B **47** 935–49
[16] Bordat P and Brown R 1999 *Chem. Phys.* **246** 323–34
[17] Keen D A, Gutmann M J and Wilson C C 2006 *J. Appl. Crystallogr.* **39** 714–22
[18] Metropolis N, Rosenbluth A W, Rosenbluth M N, Teller A H and Teller E 1953 Equation of state calculations by fast computing machines *J. Chem. Phys.* **21** 1087–92
[19] Reid J, Moore M and MacNay L 2007 *Acta Crystallogr.* A **63** 380–6
[20] Welberry T R 2004 *Diffuse X-Ray Scattering and Models of Disorder* (*IUCr Monographs on Crystallography*) (Oxford: Oxford University Press)
[21] Cailleau H, Girard A, Moussa F and Zeyen C M E 1979 *Solid State Commun.* **29** 259
[22] Cailleau H and Dworkin A 1979 *Mol. Cryst. Liq. Cryst.* **50** 217–21
[23] Almenningen A, Bastiansen O, Fernholt L, Cyvin B N, Cyvin S J and Samdal S 1985 *J. Mol. Struct.* **128** 59–76
[24] Tsuzuki S, Uchimaru T, Matsumura K, Mikami M and Tanabe K 1999 *J. Chem. Phys.* **110** 2858–61
[25] Uchida K, Kakei T and Takahashi Y 1997 *J. Lumin.* **72–74** 501–2